Gesellschaft für Anlagen- und Reaktorsicherheit (GRS) mbH

Preliminary Investigations for the Characterization and Selection of a Test Field for a Two-Phase Flow Experiment in the Äspö Hard Rock Laboratory

GRS - 145

Gesellschaft für Anlagen-
und Reaktorsicherheit
(GRS) mbH

Preliminary Investigations for the Characterization and Selection of a Test Field for a Two-Phase Flow Experiment in the Äspö Hard Rock Laboratory

D. Flach, N. Jockwer,
H. Kull, M. Komischke,
T. Rothfuchs

Dezember 1997

GRS - 145
ISBN 3-931995-03-8

Anmerkung:

Dieser Bericht ist von der GRS im Auftrag des BMBF im Rahmen des Vorhabens „Voruntersuchungen zur Gebirgscharakterisierung und Auswahl eines Versuchsfeldes für ein 2-Phasenfluß-Experiment im Äspö-Hartgesteinslabor“ erstellt worden. Der Auftraggeber behält sich alle Rechte vor. Insbesondere darf dieser Bericht nur mit seiner Zustimmung zitiert, ganz oder teilweise vervielfältigt werden bzw. Dritten zugänglich gemacht werden. Der Bericht gibt die Auffassung und Meinung des Auftragnehmers wieder und muß nicht mit der Meinung des Auftraggebers übereinstimmen.

Foreword

The German Bundesministerium für Bildung, Wissenschaft, Forschung und Technologie (BMBF) started its participation in the Äspö Hard Rock Laboratory (HRL) programme in the summer of 1995.

The investigations in the Äspö HRL are being carried out as a precaution, in addition to the research in Germany for final disposal in a salt formation; the purpose is to complete the knowledge on other potential host rock formations. The work is concentrated on investigations related to groundwater flow, radionuclide transport and geochemistry, on two-phase flow investigations, as well as the development and testing of instrumentation and methods for underground rock characterization.

Four research institutes are performing the work on behalf of BMBF: The Bundesanstalt für Geowissenschaften und Rohstoffe (BGR), the Forschungszentrum Karlsruhe/Institut für Nukleare Entsorgungstechnik (FZK/INE), the Gesellschaft für Anlagen- und Reaktorsicherheit/Fachbereich Endlagersicherheitsforschung (GRS/ESF), and the Technical University of Clausthal-Zellerfeld (TUC).

This report describes the work carried out by the GRS in 1996. The work has been concentrated on preliminary investigations for the characterization and selection of a test field for a two-phase flow experiment in the HRL.

Table of Contents

Page

List of Figures

Page

List of Tables

Page

1 Introduction

In repositories for nuclear waste in deep geological formations, gases will be present. Sources for gas production are natural degassing of the host rock, corrosion of container materials, and radiolysis. The migration of contaminated gases from the repository to the biosphere as well as the possible increase of gas pressure and its influence on the integrity of the repository are important issues in long-term safety analyses.

Gas transport out of the repository disposal areas may occur because complete backfilling of the storage rooms is hardly achievable. Potential pathways for the gases are the (moist) rock formations around the disposal areas, the excavation-disturbed zones (EDZ) around drifts and rooms, and the geotechnical barriers inside the repository. If liquids (water or brines) are present in pores or fractures, the process of two-phase flow (TPF) in the rock mass and in the seals has to be considered.

In the Äspö HRL, issues relevant to the repository are investigated by international cooperations. BMBF-funded R&D activities are concentrated on the investigation of gas propagation in moist hard rock formations, as well as an experiment concerning two-phase flow. The necessary research work was discussed between SKB, BMBF, and candidate German research institutions in January 1996. In accordance with this discussion, preliminary investigations have been performed in 1996 by GRS/ESF. Besides the testing of appropriate measurement methods and devices, the work was concentrated on the selection and preliminary characterization of a suitable test field in the mine for conducting the envisaged experiment.

2 Objectives

In order to prepare the planned TPF experiment to be carried out from 1997 to 1999, the local conditions in the near field of the underground drifts were determined, and different measurement methods were tested to estimate their suitability under the Äspö-specific conditions.

The work comprised:

- measurement of the gas content of the rock mass and of the formation water, as well as the distribution and propagation of the gas, respectively, by taking samples from sealed boreholes and from the mine air,

- determination of the extension of the excavation-disturbed zone (EDZ) by applying a new combined geoelectric method, and measurement of the moisture distribution in the EDZ and in the undisturbed rock mass, respectively,

- mapping of water-bearing structures and of their spatial distribution by measuring the characteristic drift surface temperatures.

On basis of the results of the aforementioned work, a test field for the TPF experiment was selected.

3 Preliminary site investigations and testing of measurement methods

3.1 Gas release

For determining the gas release from the granitic rock, samples of the mine air with and without ventilation and samples of the formation water from different sealed boreholes were taken. These samples were analyzed for their gas content and gas composition at the GRS laboratory in Braunschweig.

3.1.1 Gases released into the mine air

In order to determine the continuous gas release from the host rock, samples of the mine air were taken at 9 different locations of the access drift, beginning near the entrance at tunnelmeter 120 down to tunnelmeter 3599.7. To separate the influence of the diesel exhaust from the machines and cars, samples of the mine air were taken on Friday, August 9, 1996 after continuous ventilation during a five-day period, and on Monday, August 12, 1996 after the ventilation had been switched off for about 60 hours.

Additional air samples were taken at the exhaust of the mine ventilation system on Friday before switching off the ventilation, and on Monday, 0.25, 0.5, 1.0, 1.5, 2.0, and 24 hours after switching on the ventilation again. For comparison, samples of the air entering the mine were taken on August 9, 12, and 13, 1996.

The air samples were taken with a manual pump and transferred into Linde gas bags for transport to the GRS laboratory in Braunschweig to be analyzed by gas chromatography.

Table 3.1-1 summarizes the measured results.

It was found that the oxygen and nitrogen concentrations were comparable with the atmospheric concentrations. Only carbon dioxide and methane were measured in concentrations significantly above the detection limit of the gas chromatograph.

The carbon dioxide concentration during ventilation was between 350 and 527 vpm (1 vpm = 1 cm^3 / m^3) except in the region between tunnelmeter 2074 and 3200 (ZEDEX area) where up to 925 vpm were measured. Without ventilation the highest carbon dioxide concentrations

were measured in the region between tunnelmeter 120 and 675 (758 and 986 vpm) and between tunnelmeter 1730 and 2074 (959 and 808 vpm).

Methane during ventilation was measured only in the region between tunnelmeter 120 and 675 in a concentration of 3 vpm. In the deeper region the concentration was almost zero. Without ventilation a methane concentration of 32 vpm was measured in the region of tunnelmeter 675 and between 9 and 18 vpm in the region below tunnelmeter 1730. At tunnelmeter 1229 no methane was detected; the reason is not known.

From the results of the carbon dioxide and methane concentration measurements, it can be concluded that a correlation between both components exists, because methane can be oxidized by microbes if oxygen is present.

Tables 3.1-2a and 3.1-2b show the concentrations of carbon dioxide and methane in air samples taken at the mine exhaust on Friday before switching off, and on Monday after switching on the ventilation. In addition, samples of the air entering the mine were taken. The carbon dioxide concentration in the air entering the mine ranges between 350 and 380 vpm, whereas the methane concentration is below the detection limit. The air leaving the mine after continuous ventilation and an active mine period of 5 days shows a carbon dioxide content of about 380 vpm and a methane content of about 0.3 vpm. After a period of 60 hours without any ventilation, the concentration of carbon dioxide was about 500 vpm (an increase by 120 vpm), and that of methane was about 10 vpm. With ventilation both concentrations decreased, and after 24 hours they were almost at the same level as that observed during continuous ventilation.

The measurements indicate that during ventilation the operation of cars and machines does not significantly affect the concentration of carbon dioxide and methane in the mine air. However, without ventilation for 60 hours the gas concentrations increased as follows:

carbon dioxide from 369 to 492	=	123	vpm
methane by about	~	10	vpm.

Under consideration of

a mine volume of	150 000	m^3
and a surface of the galleries of	120 000	m^2 /ZEL 96/

during 60 hours about

$$150\,000 \cdot 123 \cdot 10^{-6} = 18.5\ m^3 \quad \text{of carbon dioxide and}$$
$$150\,000 \cdot \ 10 \cdot 10^{-6} = \ 1.5\ m^3 \quad \text{of methane}$$

are released. Accordingly, the release rates into the mine amount to:

7.4 m^3/d for carbon dioxide and
0.6 m^3/d for methane

representing a specific rate of

0.06 $l/(m^2 \cdot d)$ for carbon dioxide and
0.005 $l/(m^2 \cdot d)$ for methane.

This specific rate is higher in some regions by a factor of about 3 to 10. A correlation between the gas release and the mineralogy, stratigraphy, fissures, or tectonically fractured zones is rather likely.

Table 3.1-1 Carbon dioxide and methane concentration in the mine air on Aug. 9, 1996 with ventilation and on Aug. 12, 1996 without ventilation

Sampling date	Aug. 9, 1996 with ventilation		Aug. 12, 1996 without ventilation	
Tunnelmeter in the mine	CH_4 vpm	CO_2 vpm	CH_4 vpm	CO_2 vpm
120 m	2,201	437,767	4,958	758,226
675 m	3,364	481,048	32,446	986,789
1229 m	1,734	427,355	0,000	440,195
1730 m	1,087	527,794	18,867	959,813
2074 m	0,977	925,415	13,780	808,737
2783 m	0,503	664,646	12,198	604,853
3200 m+ ZEDEX	0,270	668,307	11,621	632,279
3400 m	0,000	350,004	9,230	525,034
3599,7 m	0,615	353,873	15,376	512,794

Table 3.1-2a Carbon dioxide and methane concentration in the mine air at the mine exhaust

Sampling date	Ventilation	CH_4 vpm	CO_2 vpm
Aug. 9, 1996	on	0,194	364,621
	off for 60 hours Time after switching on, h		
Aug. 12, 1996	0,25	9,356	492,155
Aug. 12, 1996	0,5	9,663	485,884
Aug. 12, 1996	1	5,172	437,771
Aug. 12, 1996	1,5	2,861	403,794
Aug. 12, 1996	2	1,713	398,373
Aug. 13, 1996	24	0,170	363,716

Table 3.1-2b Carbon dioxide and methane concentration in the air at the mine entrance

Sampling date	Ventilation	CH_4 vpm	CO_2 vpm
Aug. 9, 1996	air entering the mine	0,000	353,520
Aug. 12, 1996		0,000	369,318
Aug. 13, 1996		0,000	372,822

3.1.2 Gas content of formation water

Water samples were taken from different boreholes on June 20 and August 12, 1996. Gastight glass containers with a volume of about 500 ml were used. In the GRS laboratory in Braunschweig the containers had been prepared by flooding one half with helium and the other half with nitrogen, in order to determine hydrogen, helium, and nitrogen in the formation water. From each borehole two samples were taken with the use of both containers, with helium and nitrogen in the residual volume. For taking the water samples the valve of the borehole packer was opened, and the tube and the valve of the system were rinsed with about 2 liters of water. The glass container was then connected to the packer outlet, and the container valve was opened. 250 ml of borehole water was allowed to flow into the glass container without any contact with the mine air. The gas in the container was pressurized by the inflowing water. By carefully opening the other valve of the container, the pressure was reduced to atmospheric pressure.

The gastight containers filled one-half with water and one-half with helium or nitrogen were transferred to the GRS laboratory in Braunschweig for storage at 20 °C. Two weeks after sampling, gas was taken from the residual volume through the septum by means of a syringe. This gas was injected into a gas chromatograph for analysis.

Afterwards the gastight containers were heated to 75 °C for 24 hours to release the gases still dissolved in water. Gas was then again taken with a syringe through the septum and analyzed.

50 ml of concentrated hydrochloric acid were added to some of the water samples (from boreholes HA1960A, SA2273A, SA2600A, SA2783A, SA2880A, and SA3045A with nitrogen in the residual container volume), in order to drive out and generate further gases.

The results of these tests are shown in Tables 3.1-3 to 3.1-5. The samples from boreholes SA and HA were taken on June 20, 1996, and those from the boreholes with the designation KA on August 12, 1996.

The following gases have been identified:

1. **Hydrogen.** Up to 5.9 µl / g of water were released at 20 °C, and up to 5.6 µl / g of water at 75 °C. An exception resulted for borehole SA2880A with 80 and 74 µl / g water, respectively.
   Hydrogen could be determined only in those containers with nitrogen in the residual volume.

2. **Methane.** Up to 2 µl / g of water were released at 20 °C and, in addition, up to 2 µl / g at 75 °C (borehole KA 2511A:2). Methane could be determined in both containers with helium and nitrogen in the residual volume
   The results obtained from these different containers differ with two exceptions within the range of inaccuracy of 30 %. The inaccuracy is caused by sampling, preparation, and analysis. Since the results of the two independent measurements vary within the range of inaccuracy, the methods of sampling and analysis are correct.

3. **Carbon dioxide.** Up to 7.4 µl / g of water were released at 20 °C (borehole KA2512A) and up to 19 µl / g at 75 °C (borehole SA1229A). Carbon dioxide could be determined in both containers with helium and nitrogen in the residual volume.
   The results obtained from these different containers differ with two exceptions within the range of inaccuracy of 30 %. The inaccuracy is caused by sampling, preparation, and analysis. Since the results of the two independent measurements vary within the range of inaccuracy, the methods of sampling and analysis are correct.

4. **Ethane** was found in a few water samples. The concentration was always near the detection limit of about 0.0001 µl / g for the gas chromatograph.

Nitrogen was not found in the containers with helium in the residual volume above the detection limit of about 0.0001 µl / g of water. That means that the formation water contains no significant amounts of dissolved nitrogen.

Other gases like **helium** or **further hydrocarbons** were not found above the detection limit of about 0.0001 µl / g of water.

For releasing the gases still dissolved in the water, hydrochloric acid was added to the containers by means of a syringe.

After injecting hydrochloric acid into the water, up to 35 µl carbon dioxide per g of water were released. Samples from which large volumes of carbon dioxide had been released at 20 and 75 °C also released a large volume of carbon dioxide after the addition of hydrochloric acid. In addition, up to 0.57 µl methane per g water have been released.

3.1.3 Conclusions

The investigations show that hydrogen, methane, and carbon dioxide are dissolved in the formation water, but only methane and carbon dioxide were found in the mine air.

The distribution of the dissolved gases and their release are very heterogeneous and vary by a factor of at least 10 within the mine. The possible correlation of higher gas contents with mineralogy, stratigraphy, existing fissures, or tectonically fractured zones has not yet been investigated. Further investigations concerning this subject are considered necessary.

As far as two-phase flow experiments in granite are concerned, this investigation shows that gases stored in the granite or dissolved in the formation water have to be taken into account.

Table 3.1-3 Gas release from the water of different boreholes at 20 °C

Water from borehole	Gas in the residual volume of the sampling container						
	Nitrogen				Helium		
	H_2 [1)] µl/g	CH_4 µl/g	CO_2 µl/g	C_2H_6 µl/g	CH_4 µl/g	CO_2 µl/g	C_2H_6 µl/g
SA1009B	0,009	0,374	2,767		0,394	3,068	
SA1229A		0,770	0,336		0,845	4,996	
SA1420A	0,003	0,629	0,652		1,338	1,166	
SA1730A		0,308	0,534	0,00022	0,326	0,666	
HA1960A	1,065	0,282	0,187		0,472	0,631	
SA2074A	1,210	0,874	0,873		0,955	0,980	
SA2273A	0,506	0,390	1,740		0,335	1,691	
SA2600A	0,044	1,165	0,999	0,00013	1,737	1,270	
SA2783A	5,969	0,048	0,103	0,00011	0,047	0,084	0,00013
SA2880A	80,559	0,075	0,063	0,00013	0,115	0,161	0,00018
SA3045A	1,054	0,021	0,063		0,024	0,122	
HA3289B		0,172	0,935		0,170	0,867	
KA2511A:2		2,075	4,260		1,878	3,789	
KA2512A		1,726	7,402		1,968	7,260	
KA2558A:2		0,017	0,172	0,00012	0,010	0,099	0,00010
KA2862A:1		0,016	0,105	0,00018	0,022	0,065	0,00027
KA3010A:2		0,045	0,203		0,051	0,201	
KA3067A:3		0,329	0,618		0,312	0,425	
KA3105A:3	0,024	0,483	1,617		0,471	1,488	
KA3105A:4	0,110	0,392	2,739		0,435	2,935	
KA3110A:1		0,461	1,642		0,416	2,200	
KA3385A:1		0,085	0,079		0,076	0,103	

[1)] Hydrogen could be determined only in the container with nitrogen in the residual volume.

Table 3.1-4 Gas release from the water of different boreholes after tempering for 24 hours at 75 °C

Water from borehole	Gas in the residual volume of the sampling container						
	Nitrogen				Helium		
	H_2 [1)] µl/g	CH_4 µl/g	CO_2 µl/g	C_2H_6 µl/g	CH_4 µl/g	CO_2 µl/g	C_2H_6 µl/g
SA1009B		0,309	13,400		0,325	9,128	
SA1229A		0,524	5,939		0,764	19,018	
SA1420A		0,462	2,465		0,934	5,141	
SA1730A		0,264	1,901		0,293	2,291	
HA1960A		0,241	1,317		0,162	3,372	
SA2074A	0,149	0,740	3,437		0,661	4,218	
SA2273A		0,343	12,001		0,288	11,033	
SA2600A	0,006	0,903	5,783		1,442	9,698	
SA2783A	5,612	0,043	0,695		0,043	0,593	
SA2880A	74,655	0,063	0,362	0,00008	0,096	1,032	
SA3045A	0,640	0,016	0,446		0,018	0,625	
HA3289B		0,137	3,859		0,152	4,509	
KA2511A:2		1,996	14,021		1,890	13,792	
KA2512A		1,703	11,319		2,051	11,919	
KA2558A:2		0,017	0,400	0,00011	0,009	0,300	0,00009
KA2862A:1		0,016	0,317	0,00017	0,021	0,242	0,00025
KA3010A:2		0,042	0,538		0,049	0,576	
KA3067A:3		0,308	1,798		0,312	1,598	
KA3105A:3	0,012	0,407	6,376		0,465	7,341	
KA3105A:4	0,072	0,424	5,227		0,434	6,301	
KA3110A:1		0,452	6,014		0,412	4,958	
KA3385A:1					0,086	0,294	

[1)] Hydrogen could be determined only in the container with nitrogen in the residual volume.

Table 3.1-5 Carbon dioxide and methane release from water of different boreholes at 20 °C, 75 °C, and after injection of HCl (nitrogen in the residual volume of the container)

Water from borehole	Carbon dioxide µl/g			Methane µl/g		
	20 °C	75 °C	HCl	20 °C	75 °C	HCl
HA1960A	0,187	1,317	22,318	0,282	0,241	0,166
SA2273A	1,740	12,001	33,798	0,390	0,343	0,226
SA2600A	0,999	5,783	17,179	1,165	0,903	0,572
SA2783A	0,103	0,695	3,922	0,048	0,043	0,373
SA2880A	0,063	0,362	2,164	0,075	0,063	0,061
SA3045A	0,063	0,446	2,222	0,021	0,016	0,015

3.2 Geoelectrics

The objective was the development and application of geoelectrics to selecting a test field for the planned two-phase flow experiment.

The electrical resistivity is a characteristic property of rocks. It depends on the ion mobility in the pores, which are completely or partially saturated with electrolyte containing ionic charge carriers. By determining the dependence of the electrical resistivity on the water saturation in the laboratory, one can use the electric method to indirectly investigate the water saturation of rock in situ. Because of the inhomogeneities in rocks, geoelectric field measurements yield apparent resistivities. Inverse modeling is applied for converting the apparent resistivity to a "true" model resistivity for comparison with resistivity/saturation values from laboratory measurements.

The objective of the measurements at the HRL was to test the suitability of the electric method thus developed. The method combines field measurements, laboratory calibration measurements, and inverse modeling. It was used for investigating the EDZ around two drifts excavated by a tunnel boring machine (TBM) and by drilling and blasting (D&B).

Earlier investigations /OLS 96/ of these drifts during and after excavation had been performed within the framework of the Zone of Excavation Disturbance Experiment (ZEDEX). In order to characterize the initial conditions in the rock mass, drift mapping, core logging, in situ seismic velocity measurements, and radar measurements had been carried out. The rock mass response to excavation had also been observed by mapping induced fractures. Extensometer and convergence measurements, as well as acceleration, vibration, seismic velocity, permeability, and acoustic emission measurements had been conducted in addition to laboratory investigations.

3.2.1 Method

Field measurements

Basis of the measurements is Ohm's law,
where

$$J = \sigma E.$$

J is the electric current density measured in amperes per square meter (A/m^2), E is the electric field intensity measured in volts per meter (V/m), σ is the conductivity measured in siemens per meter (S/m). The latter is the reciprocal of the resistivity ρ measured in ohms times meters (Ω m). The resistivity is the property by virtue of which a material resists the flow of electric current.

The electric field E is a scalar potential field. It is equal to a potential current produced by charged bodies. The potential has been used because it is easier to measure than the electric field.

In applied geophysics electric measurements have been used for a long time to determine the resistivities of different Earth materials. The most applicable method is a four-point method; that is, two electrodes are used to introduce current into the material, and two further electrodes are used to measure the electric potential difference caused by the induced current. Many electrode arrays have been used for measuring the resistivity of Earth materials. Here, the so-called Wenner array shown in Fig. 3.2-1 has been used.

This array consists of four equally spaced in-line electrodes. The electrode array is moved along a traverse. For every measurement cycle the electrode spacing is increased stepwise. This method is called electric sounding because the electrode spacing is increased stepwise to obtain information from greater depths at a given surface location /TEL 90/. In the Wenner array the central two electrodes are the potential electrodes, and the outer two electrodes are the current electrodes (Fig. 3.2-1). The Wenner array used here yields the resistivity,

$$\rho_a = 2\pi \frac{\Delta U}{I} a$$

The resistivity ρ_a is an apparent resistivity because of rock inhomogeneities. It is the product of the voltage-to-current ratio and a geometry-dependent weighting factor a, which is called the geometric factor. It is generally dependent on the electrode array and spacing. In the case of the Wenner array the geometric factor is equal to the electrode spacing a, which

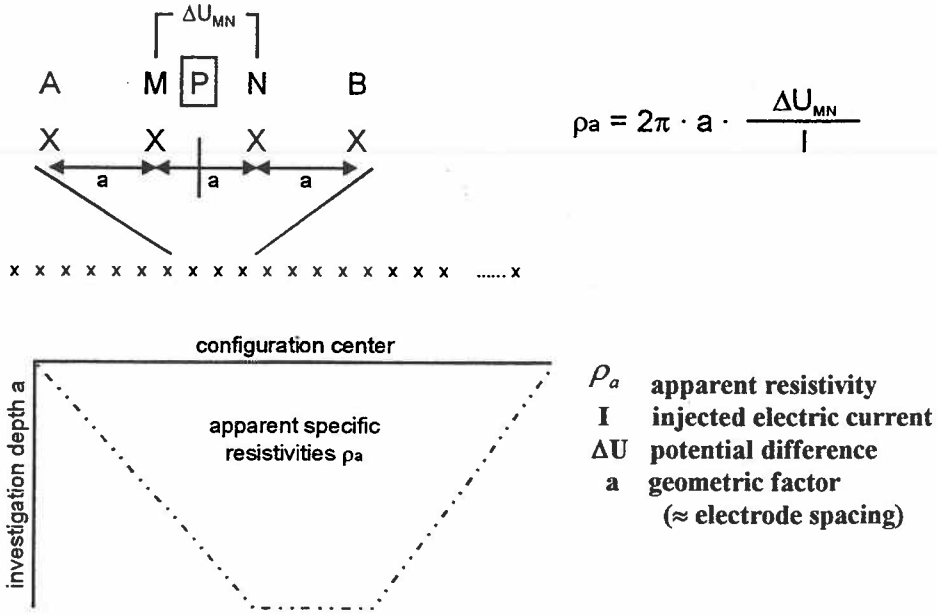

Fig. 3.2-1 Principle of geoelectric sounding using of a Wenner array

also corresponds to the depth of investigation. A plot of apparent resistivities is designated as a pseudosection and is a function of the position and electrode spacing. The pseudosection indicates how the apparent resistivity varies with location and depth.

Modeling

The measured resistivity of a geological formation is frequently an apparent resistivity because of the rock inhomogeneities which usually exist. By means of modeling, the apparent resistivity can be converted to a "true" model-dependent resistivity. For a better understanding, the following concepts are explained.

Calculating the effect of a model is called forward or direct modeling. Determining a model which could have given rise to observed effects is called inverse modeling or inversion. A model is a concept from which one can deduce effects for comparison with observations, and which is applied to develop a better understanding of observations. Agreement between observations and effects derived from a model does not prove that the model represents the actual situation. Geophysical interpretation problems almost always lack uniqueness. Where a distribution of causes produces a distribution of measured values which depend on a system of parameters, the forward problem is expressible as the matrix equation

$$M = P\,V,$$

which is also called the model. *M* is a vector of the measurements m_i, *P* is a matrix of the parameters p_{ij}, and *V* is a vector of the values v_j. Solving the equation for v_j is the inverse problem. Usually, v_j depends on the measurement system. The corresponding matrix equation for the electric inverse problem is

$$\Delta d = A\, \Delta p,$$

where Δd is the vector of differences between modeled responses and data, Δp is the correction vector to the initial model parameters p_0, and *A* is the Jacobian matrix or the matrix of the partial derivatives of the modeled response with respect to the model parameters /SAS 92/. During the past years a series of codes based on different algorithms has emerged. In the course of this project the commercially available program RES2DINV by Loke and Barker /LOK 96/ has been used.

The pseudosections and results obtained by inversion are shown for the D&B drift in Fig. 3.2-3 and for the TBM drift in Fig. 3.2-4.

Calibration measurements

It is known that the resistivity of rock can be expressed in terms of water saturation and porosity, because the electrical resistivity depends on the pore microstructure and the resistivity of the pore content. Archie`s empirical formulas express the relationships between formation factor *F*, porosity Φ, water saturation S_w, and true resistivity R_t /ARC 42/:

$$F = R_0 / R_w = \Phi^m,$$

$$R_0 / R_t = S_w^n,$$

where *m* = cementation factor, which varies between 1.3 and 3.0,

R_0 = resistivity of the formation when 100 % saturated with formation water,

R_w = resistivity of the formation water,

R_t = true resistivity of the formation,

n = saturation exponent, which is often between 1.5 and 2.5.

The exponents *m* and *n* are approximately constant for given rock type. By solving both equations for R_0 and equating, we obtain

$$R_w \Phi^m = R_t S_w^n ,$$

and thus:

$$R_t = R_w \Phi^{-m} S_w^{-n} .$$

If the parameters R_w and Φ as well as the exponents *m* and *n* are determined by laboratory measurements, the relationship between the true resistivity of the rock formation and water saturation can be presented on a calibration diagram /YAR 92/.

The laboratory calibration measurements could not be performed during this preliminary phase of the project, because they would have required too much time. It is intended to deal with them at a later stage of the project.

3.2.2 Field measurements

The electric measurements at HRL were performed on profile lines in two different drifts. The locations of the profile lines can be seen in Fig. 3.2-2. The profile line in the D&B drift is 20 m long on the south wall, 1.4 m above the floor. The profile line in the TBM drift is also 20 m long and is between tunnelmeter 3200 and tunnelmeter 3220, on the north wall, 1 m above the floor.

A total of 2 times 81 electrodes were installed. The measurements were started with an electrode spacing of 0.25 m, which was increased stepwise by 0.25 m after every measurement cycle. This method is called electric sounding. The geoelectric measurement system used was a commercially available SYSCAL-R2. The field measurements were conducted on May 28 and 29, 1996.

3.2.3 Results from field measurements

The results of measurements in the D&B drift are presented in Fig. 3.2-3. The increase in resistivity towards the surface in the inverted section is evident (B). This area can be interpreted as the excavation-disturbed zone ranging between several decimeters in the center and 2.5 m at the margins. At a depth of about 3.5 m there seems to be a zone with a higher water content (A), which cannot be completely analyzed because of the limited penetration depth of the electric method. The lateral anomalies on the surface along the

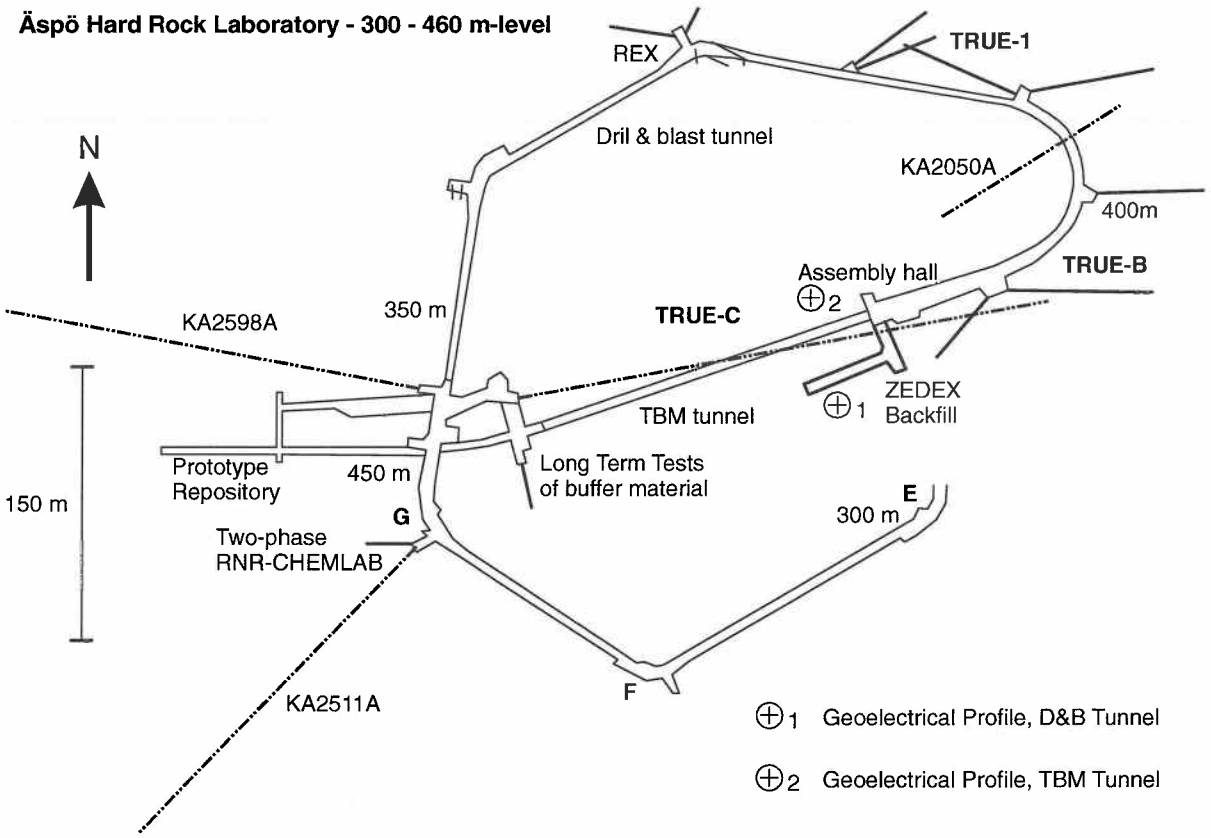

Fig. 3.2-2 Locations of the geoelectrical profile lines at Äspö HRL

profile are due to wet or dry surface regions. Only a small area of "intact" rock mass can be seen (C).

The drift excavation caused a disturbed zone of very high irregularity at the surface, with varying extension. Its average extension is between 0.5 m and 2 m.

The results of measurements in the TBM drift are presented in Fig. 3.2-4. The area of intact rock mass can be separated from the other anomalies. The high-resistivity anomaly towards the surface characterizes the disturbed zone (B). Its extension varies between a few centimeters and the decimeter range. This is in contrast to the EDZ extension in the D&B drift, which is between 0.5 m and 2 m deep on the average. A large anomaly of low resistivity correlates well with a water-bearing fracture at this location (A), which seems to disappear at a depth of about 1.5 m. In good agreement with the results in the D&B drift given above, the resistivities are up to 10^4 Ωm in the disturbed zones and up to 10^3 Ωm in the intact rock mass (C).

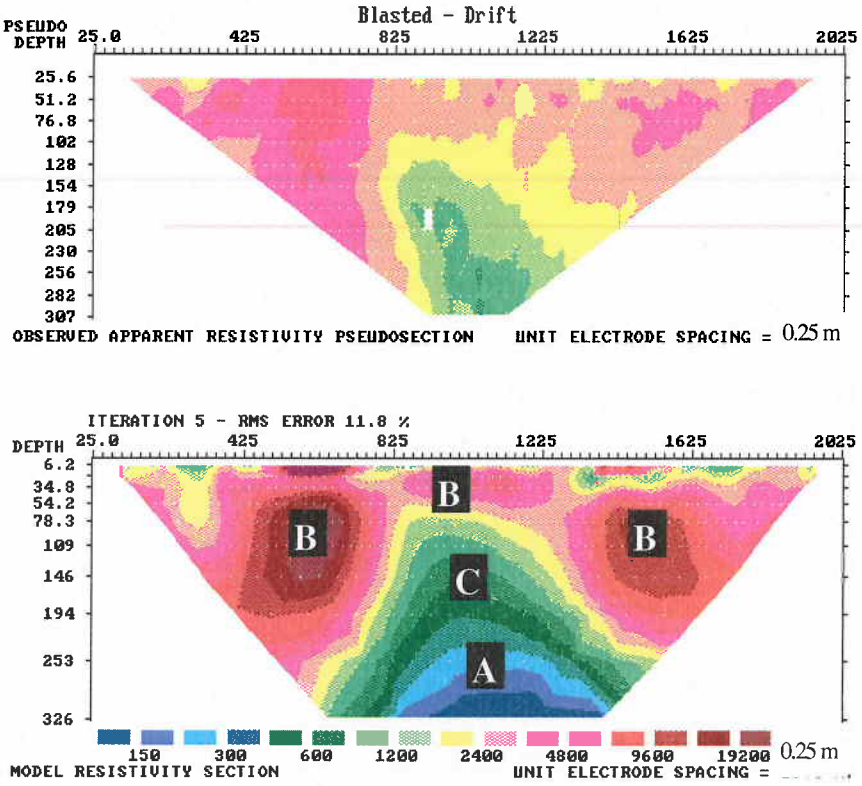

Pseudosection
(observed apparent resistivities [Ωm])

Inverted Section
(model calculated resistivities [Ωm])

Fig. 3.2-3 Results from geoelectrical measurements in the D&B drift. Coordinate axes in cm. A: fractured water-bearing area, B: excavation-disturbed area, C: intact rock mass.

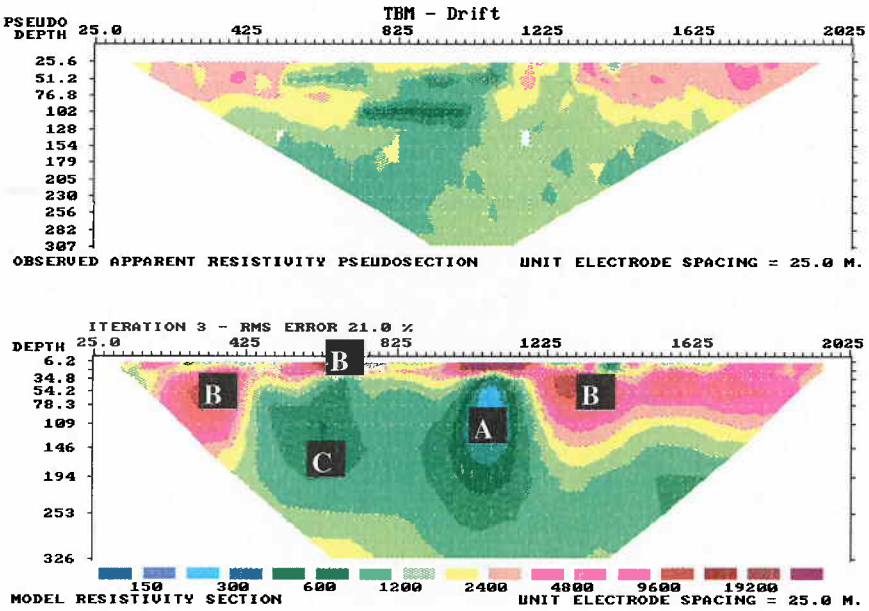

Pseudosection
(observed apparent resistivities [Ωm])

Inverted section
(model calculated resistivities [Ωm])

Fig. 3.2-4 Results from geoelectrical measurements in the TBM drift. Coordinate axes in cm. A: water-bearing fracture, B: excavation-disturbed zone, C: intact rock mass.

3.2.4 Conclusions

Since the EDZ is assumed to be a desaturated zone around a drift, which gives rise to TPF-phenomena, geoelectric measurements were performed to investigate the extensions of the EDZ around two drifts which had been excavated either by TBM or by D&B. The reason for utilizing an electric method is the dependence of the electrical resistivity of rocks on porosity and water saturation.

If one looks at the results from both drifts, it can be concluded that lateral inhomogeneities near the surfaces are due to different wetting of surface regions. The results differ by the apparently more severe disturbance and greater extension of the EDZ around the D&B drift than for the EDZ around the TBM drift.

If the resolution of the electric measurements is taken into consideration, the resistivities in different regions are almost equal. In both drifts, the resistivities after inversion are about 10^4 Ωm in the EDZ and about 10^3 Ωm in the so-called intact rock, with a saturation of 100 percent.

3.3 Thermography

The objectives of the infrared temperature measurements were

- mapping of hydraulic conductive features in tunnels excavated by different methods,
- characterization of homogeneous rock areas as part of the test field selection,
- testing of the suitability of this method in wet underground facilities.

In order to investigate the suitability of the thermographic method under the HRL conditions, temperature measurements were performed in the D&B drift and in the TBM drift at tunnelmeter 3200 to 3220 and in the access shotcrete tunnel between tunnelmeter 1316 and 1346 (area of NE-1). In addition, the method was applied in the niche at tunnelmeter 3170 and in the niche at tunnelmeter 2715 to determine the temperature field at the surfaces of these niches, which had been proposed for conducting the two-phase flow experiment.

It should be noted that the infrared method is usually applied under ambient conditions with low relative humidity, because of the influence of ventilation on the temperature distribution at rock surfaces. Very little experience has been gained with high relative humidity and moist rock surfaces, for instance at the HRL. However, the identification of water-bearing fractures by thermography is possible when the temperatures of the formation water and rock matrix are different. In the case of evaporation effects, the temperature measurements can also provide information on areas of low hydraulic conductivity.

3.3.1 Method

The temperature measurements were performed with the use of the mobile thermography tool AGEMA Thermovision 900. The system consists of the scanner with different types of lenses, the system controller, a VGA monitor, and a printer (Fig. 3.3-1). As far as underground application of the system is concerned, the only restrictions are due to climatic conditions. The operating temperature should be between -15 °C and +55 °C, and the system should be protected against extreme humidity.

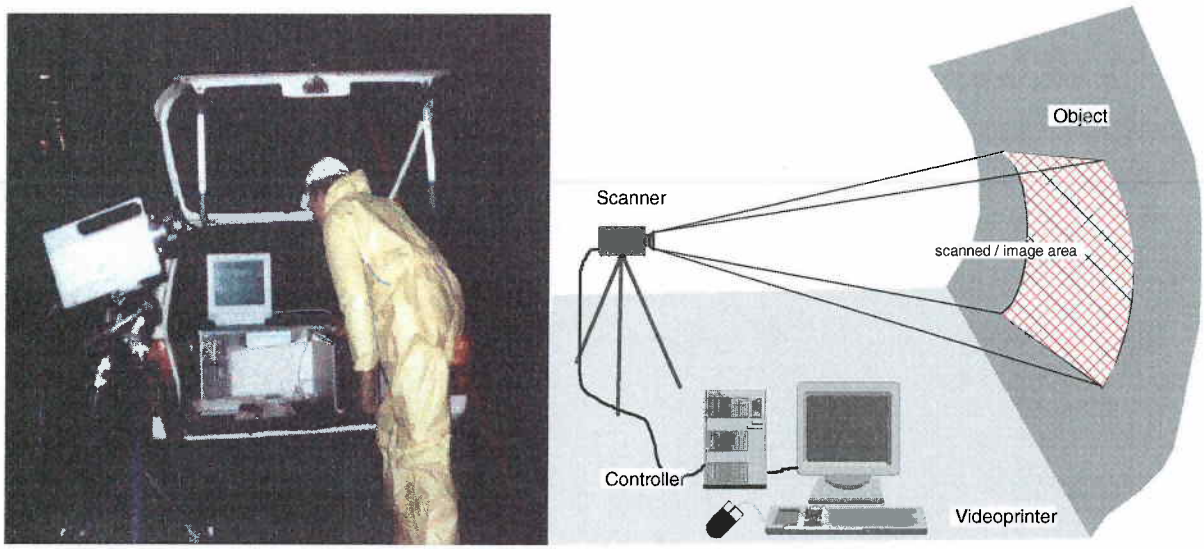

Fig. 3.3-1 Mobile thermographic system employed at a wet underground location. Scheme of thermographic measurements.

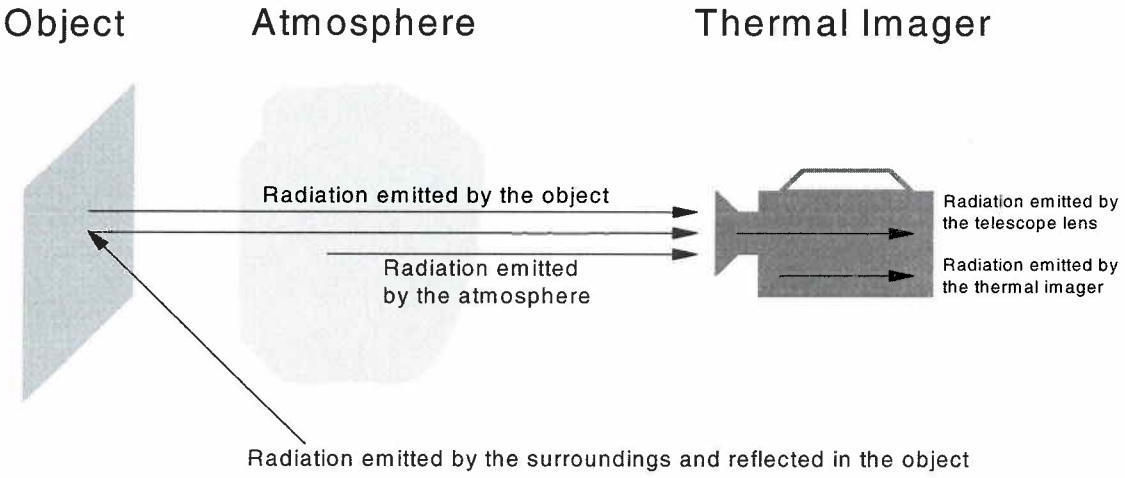

Fig. 3.3-2 Scheme of radiation emitted by objects, atmosphere, and surroundings.

The scanner is a thermographic camera which operates opto-mechanically and measures the total electromagnetic radiation in the infrared (thermal) range from 2.0 to 5.4 µm. Usually, each material (solid, liquid, gas) emits infrared radiation as a function of its temperature. In correspondence with the translucent behavior of the material, the radiation is transmitted, absorbed or reflected (Fig. 3.3-2). The measured total radiation from the rock surfaces includes the transmitted radiation of features at different temperatures and the reflected radiation which is not absorbed by the atmosphere. The total radiation is a measure of the temperature of the scanned area. The size and resolution of the scanned area depend on the distance between the scanner and the rock surface.

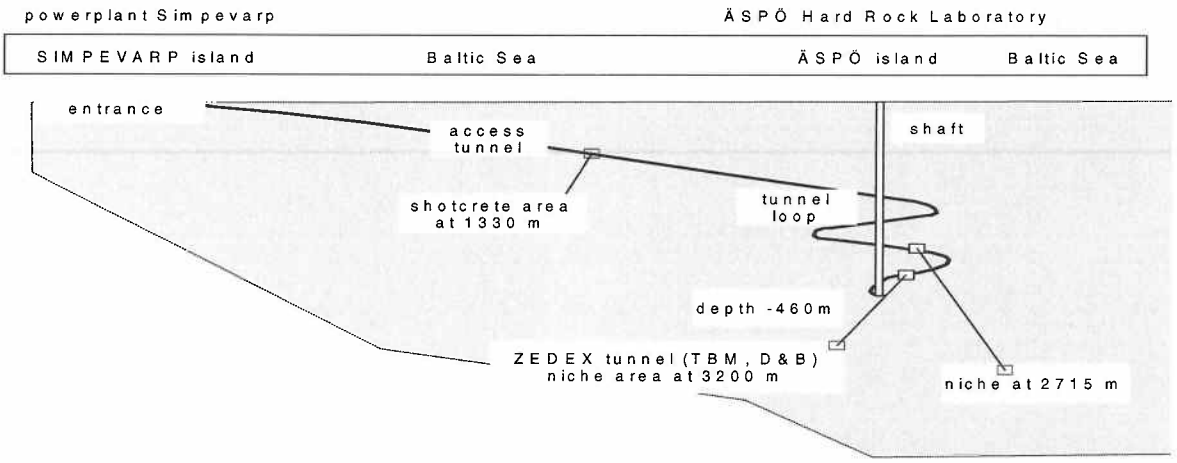

Fig. 3.3-3 Vertical section of the drift and shaft system at the ÄSPÖ HRL, showing the locations of thermographic measurements. The designated test location for the planned TPF experiment is situated at a distance of 2715 m from the tunnel entrance.

The temperature calibration of the scanner system is carried out with internal black-body radiators at a constant known temperature. The measured temperature data are taken as a 128*204 value frame (lines and rows of the temperature image). They are linked with internal calibration parameters and with external information such as the date, time, ambient temperature, air temperature, relative humidity, object distance, scanner type, lens type, filters, and individual comments. The complete data set is stored as a single image or sequence of images in a file. The results are printed as hardcopies in the form of coloured temperature maps. For data processing, the OS9-Agema-Software Erika or the PC-Windows-Agema Software IrWin must be used.

3.3.2 Results from field measurements

The temperature distribution on the rock surface was measured at five underground locations inside the HRL (compare chapter 3.3). To avoid effects of external radiators (such as underground motor vehicles), the measurements were performed when the tunnel system was closed to transportation activities. The temperatures of the atmosphere and the rock mass were measured separately by a PT-100 probe. The selected locations for temperature measurements are presented in Fig. 3.3-3. Each location is represented by a temperature image, as shown in Figures 3.3-4 to 3.3-7. The mean temperature data and ambient climatic conditions are shown in these Figures too.

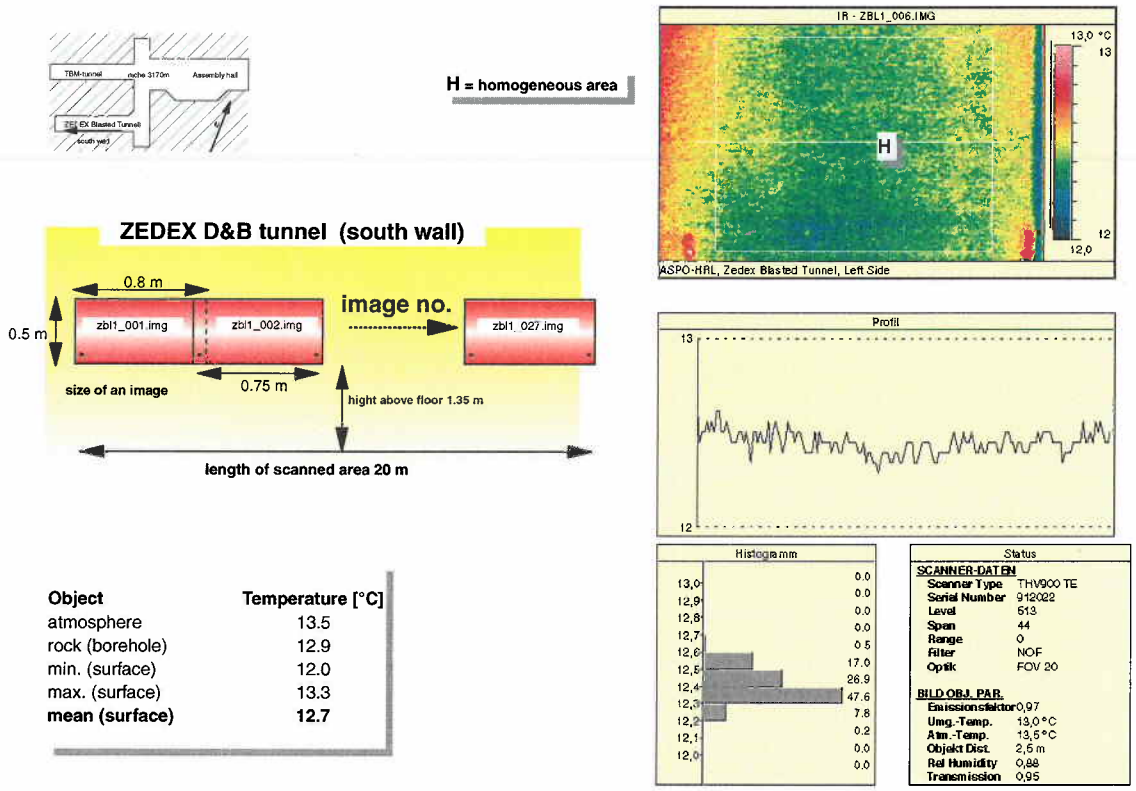

Object	Temperature [°C]
atmosphere	13.5
rock (borehole)	12.9
min. (surface)	12.0
max. (surface)	13.3
mean (surface)	**12.7**

Fig. 3.3-4 Position and temperatures of thermographic scan areas at the south wall of the D&B drift (left). Representative thermographic image measured in the D&B drift (right).

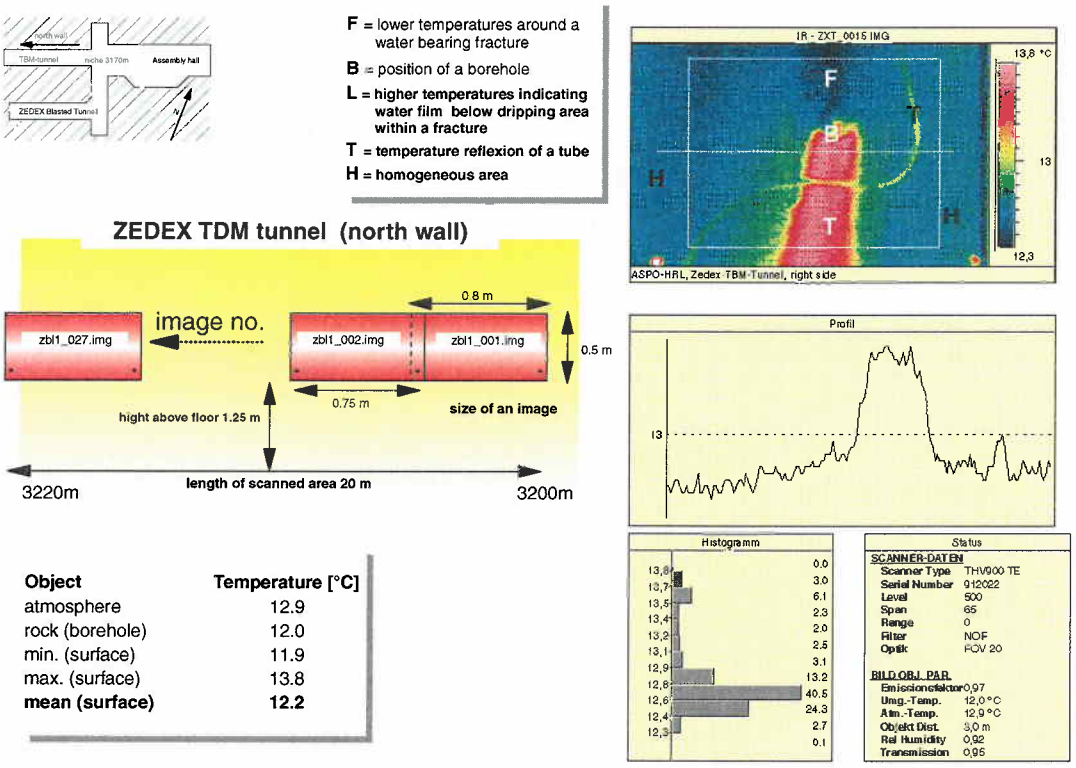

Object	Temperature [°C]
atmosphere	12.9
rock (borehole)	12.0
min. (surface)	11.9
max. (surface)	13.8
mean (surface)	**12.2**

Fig. 3.3-5 Position of thermographic scan areas at the north wall of the TBM drift (left). Thermographic image of an area representing a more highly transmissive structure in the TBM drift (right).

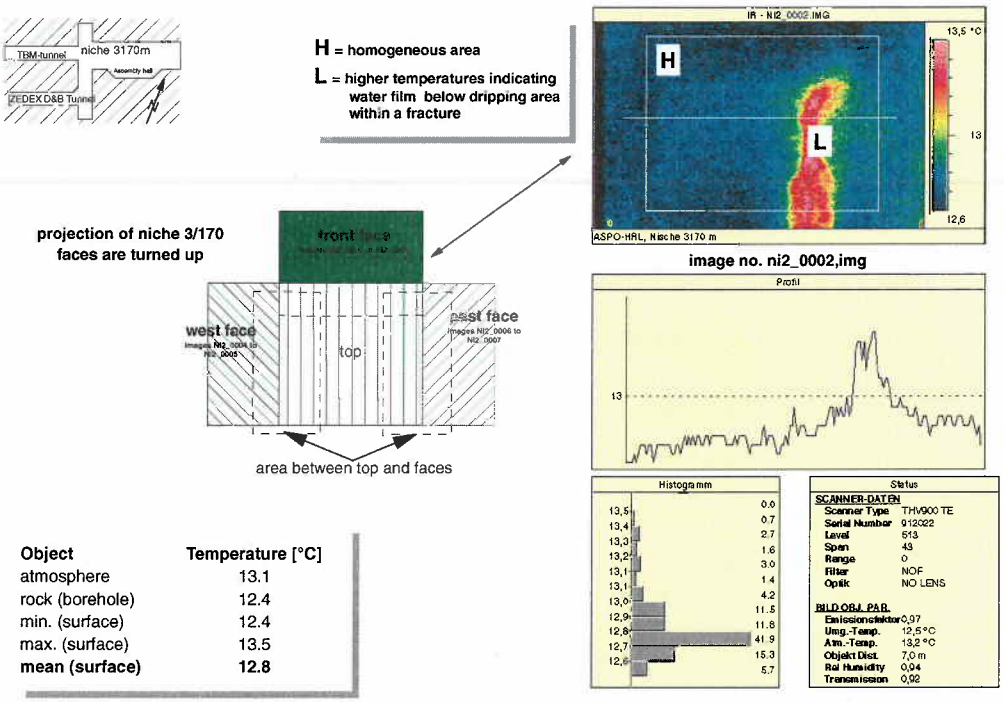

Object	Temperature [°C]
atmosphere	13.1
rock (borehole)	12.4
min. (surface)	12.4
max. (surface)	13.5
mean (surface)	**12.8**

Fig. 3.3-6 Position of thermographic scan areas in the niche at tunnelmeter 3170 (left). Thermographic image of the front (north) wall with transmissive structure (right).

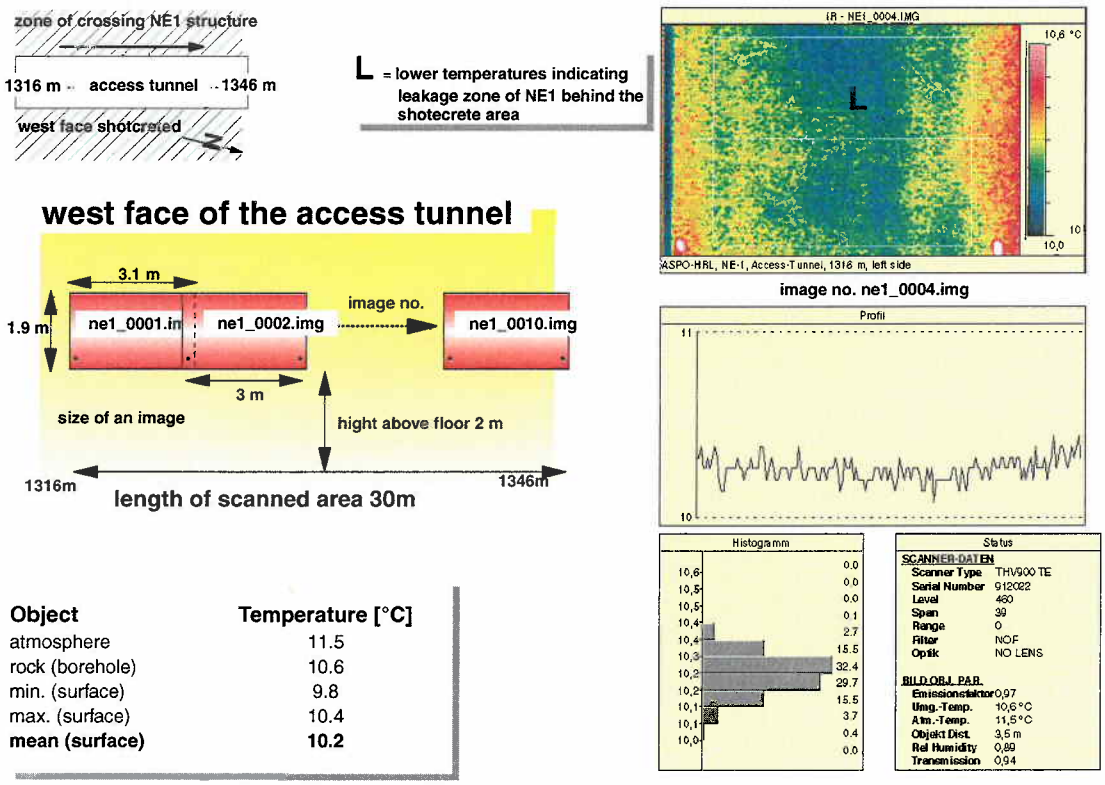

Object	Temperature [°C]
atmosphere	11.5
rock (borehole)	10.6
min. (surface)	9.8
max. (surface)	10.4
mean (surface)	**10.2**

Fig. 3.3-7 Position of thermographic scan areas at the west wall of the access tunnel between tunnelmeters 1316 and 1346 (left). Thermographic image of the shotcreted wall in the access drift (right). Temperature differences could be caused by water-bearing structures behind the concrete.

3.3.3 Data interpretation

The mean surface temperature in tunnels ranges between 10.2 and 12.7 °C. The separately measured atmospheric temperature was between 12 and 13.5 °C. A maximal temperature of 13.7 °C was measured at the TBM drift, and a minimal temperature of 9.8 °C was measured in the shotcrete area of the access tunnel.

Because of this small temperature range, as well as the accuracy of 0.1 °C of the thermographic system, the correlation of temperature distribution and rock structures should not be overemphasized (Fig. 3.3-4; image ZBL1_006). However, some information obtained from the measured data is related to the water saturation of the rock matrix.

Areas of 'higher' temperatures in the TBM drift (Fig. 3.3-5; image ZXT_0015) and in the ZEDEX niche (Fig. 3.3-6; image NI2_0002) are caused by surface reflections called 'mirror effect'. In each case, rock surfaces coated with a water film reflect the radiation from permanent lights installed at the top of the tunnel - example for external radiation. In Fig. 3.3-5 the lower temperatures above the 'warmer' area indicate a zone of the rock which is in contact with a water-bearing fracture - example for a high transmissive structure. The temperature of a tube fixed at the rock surface is influenced by the higher temperature of the atmosphere - example for ventilation effects. In the surroundings a normal temperature distribution indicates homogeneous conditions.

Other fractures which were also mapped as water-bearing structures, particularly in the niche at 2715 m, showed no significant temperature anomalies (Fig. 4.2-1; image TP1_0002). Generally, areas with a more or less relatively homogeneous temperature distribution indicate a balanced water saturation of the rock mass (Fig. 3.3-8). The increase of the mean temperature in the D&B drift is caused by the ventilation of this drift section (Fig. 3.3-9).

Except for zones with technically caused anomalies, no altered temperature areas were detected in the D&B drift.

Lowest temperatures of about 9.8 °C were measured in shotcreted areas of the access tunnel between 1316 and 1346 m, where a highly transmissive fracture intersects the tunnel (Fig. 3.3-7; image NE1_0004). Possible explanations are damaged zones in the shotcreted coating and the drainage of colder formation water.

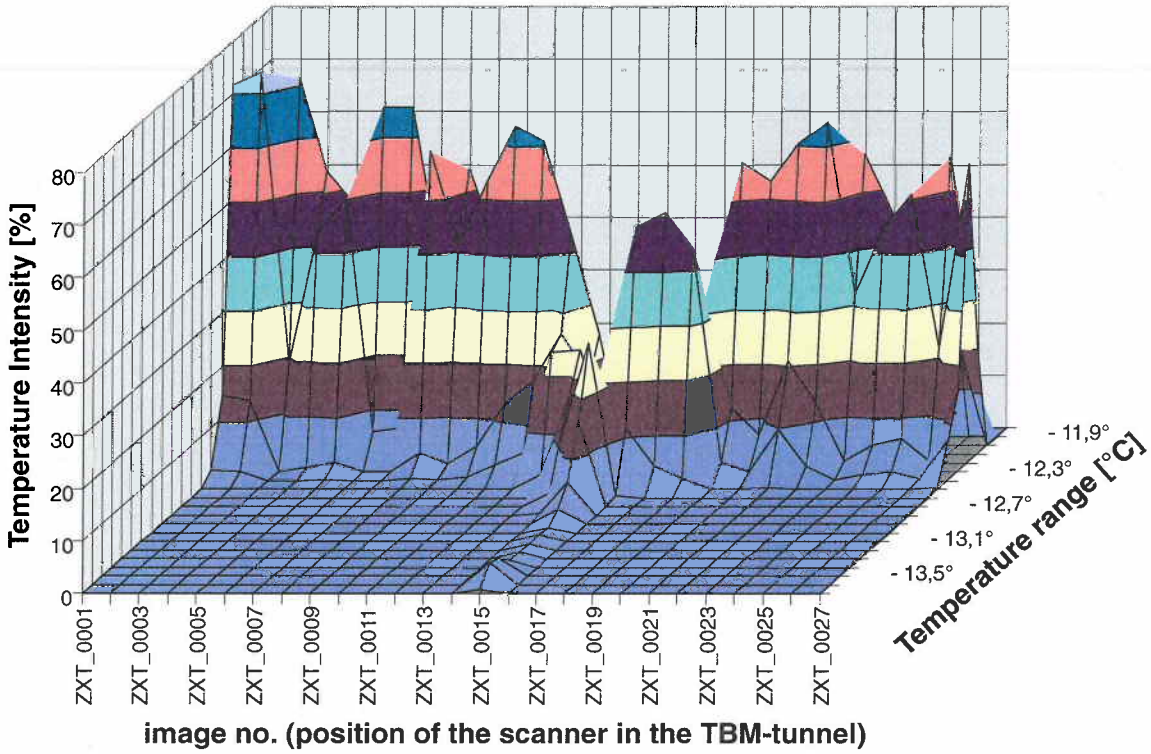

Fig. 3.3-8 Results of thermographic measurements in the TBM drift.

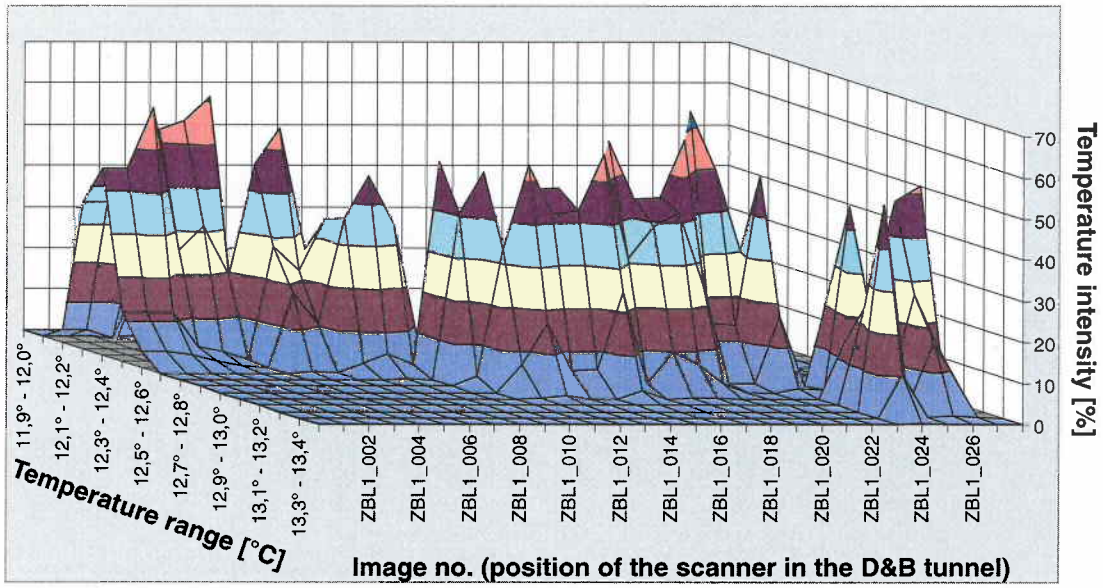

Fig. 3.3-9 Results of thermographic measurements in the D&B drift.

An obvious feature is the shift of temperature values with image numbers caused by the ventilation. In contrast to expectation, a homogeneous temperature distribution was found at some highly structured areas in the HRL. Obviously, these fractured areas do not communicate with existing highly transmissive water-bearing fractured zones. One explanation is that these fractured zones are caused by excavation techniques and reflect the damaged zone around the underground opening, rather than the natural dissection of the rock mass. At some other smooth excavated locations, however, for instance in the TBM drift, a clear correlation has been found between the temperature distribution and the fracture system.

Main points in summary:

- The surface temperature was found to be balanced and homogeneous.
- Single areas of lower temperature correlate with transmissive fractures.
- Fractured areas in the D&B tunnel and similar unfractured areas in TBM tunnel have the same temperature distribution.
- The influence of evaporation on the temperature distribution at the rock surface is less pronounced.
- The thermographic method can be used to identify hydraulically active structures even under the wet conditions found at the HRL.

4 Site selection for a two-phase flow experiment

Investigations on site evaluation for the planned two-phase flow (TPF) experiment in a fracture/matrix system were focused on the niche at the outer drift loop at tunnelmeter 2715 (Fig. 3.3-3). The preliminary decision on this test location was made for practical reasons. Preliminary investigations at other locations, such as the ZEDEX niche at tunnelmeter 3170 or the fractured drift sections of NE1, have not been performed in detail.

The test field was selected under consideration of the following criteria:

- an undisturbed and hydraulically representative rock mass,
- the precise knowledge of predominating fracture systems,
- sufficient distance from existing or planned in situ experiments, to avoid undesirable influences.

Geological and thermographic methods were used for the test field investigation.

4.1 Geological mapping

Starting at the Simpevarp island, the distance from the entrance of the access tunnel to the niche - located below the Äspö island - is 2715 m. The depth of the niche is 370 m below sea level. The ZEDEX drift is located next to the niche, at a distance of 250 m toward the deepest level. Other niches at higher levels are used for different kinds of experiments (for instance, the TRUE experiment).

The horizontal dimensions of the designated test niche are 8 m by 6 m square; its height is about 4.5 m (Fig. 4.1-1). The location was excavated by blasting. It was used for interim storage of the outcrop material. Because the blasting of the niche area was not smooth, the front face is highly disturbed. Several 'pipes' (unblasted dynamite boreholes) 50 to 100 cm long are still present in the middle of the front face. The pipes are surrounded by intensive secondary fracture systems of brittle deformations. On a macroscopic scale, 'ÄSPÖ diorite' and fine-grained granite - local name 'småland granite' - are the dominant rock types. The boundary of these two local rock types crosses the niche vertically in the south-north-direction.

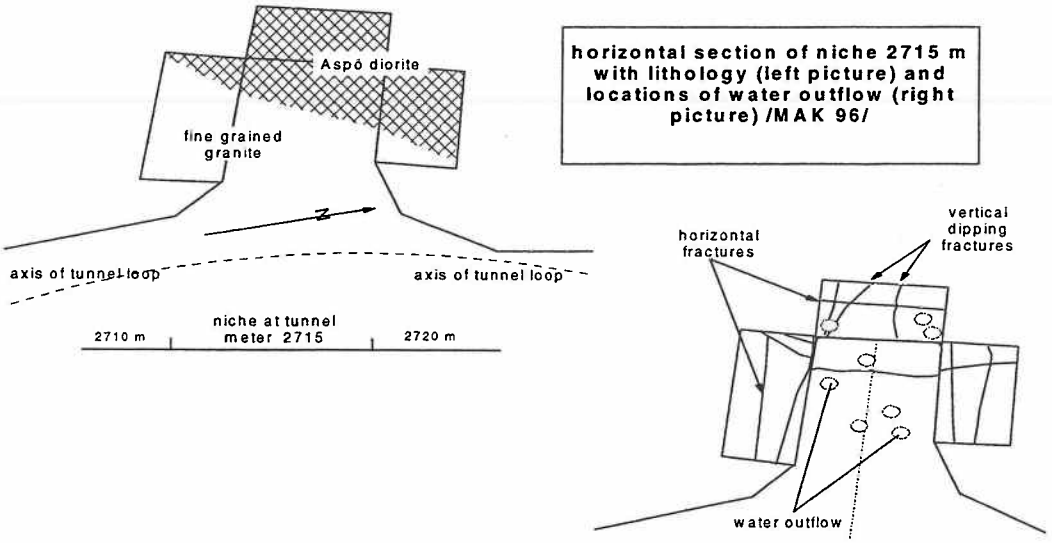

Fig. 4.1-1 Lithology and water-bearing structures determined during excavation of the niche at tunnelmeter 2715 /MAR 96/.

The axis of the niche is oriented in the east-west direction, nearly parallel to main transmissive fracture systems which dip steeply to the north-northeast. Most of the water outflow points can frequently be observed within these fractures. The orientation of other structures, for example, a second discontinuity system of flat lying fractures, is not affected. One of these horizontal fractures crosses the niche 1 m above the floor. The lateral extension of the calcite-filled fracture does not seem to be restricted. Horizontal fractures occur frequently (for instance, at the top of the niche) at vertical distances of several meters.

From a macroscopic point of view, the major fracture systems as well as the matrix areas are saturated with water.

Fig. 4.1-2 (left) shows the results from geological mapping of the rock surface at the front face. Although the geology is in reality more complex, the figure gives an impression of the major hydraulic pathways and the intersection of hydraulic structures. The front is characterized by subvertical and horizontal fractures which divide the matrix of the ÄSPÖ diorite into different blocks. The area between the major discontinuities is considered to be suited for the design of the planned two-phase flow experiment. A scheme of suggested hydraulic boundaries of the matrix/fracture system is shown in Fig. 4.1-2 (right); the

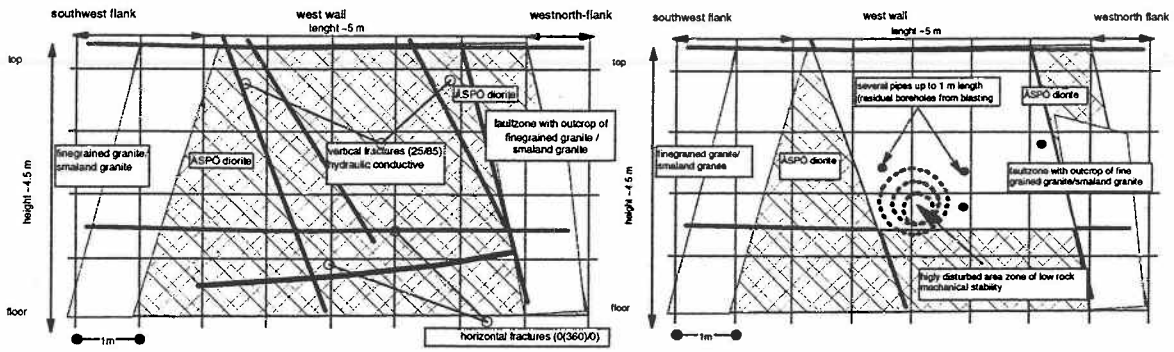

Fig. 4.1-2 Relevant lithology and hydraulic structures of the west wall (left). Transmissive boundary structures of the designated test area (right). Additional blasting is necessary to minimize the extension of the excavation-disturbed zone.

damaged zone around the pipes is neglected. Excavation of this area by smooth blasting prior to the instrumentation of the test area is proposed.

4.2 Thermography in the niche at tunnelmeter 2715

The temperature distribution on rock surfaces in the niche at tunnelmeter 2715 was determined by means of thermographic measurements in May 1996 (chapter 3.3). Figure 4.2-1 shows the geometry of the scanned area and the measured overall temperature distribution in the niche. The front face of the niche (5.9x3.6 m), the south wall and the north wall (each 3.6x2.2 m), including the transition zone to the roof, were scanned.

The measured temperature at the side walls of the niche is in the range between 11.7 and 12.5 °C. In relation to the resolution of the thermographic measurement system (+/- 0.1 °C), the temperature distribution is considered to be homogeneous. 'Warmer' areas (mean temperature plus 0.2 °C) are measured on the left side of the center and at the north wall near the floor. The only 'cold' area (mean temperature minus 0.2 °C) was found in the upper part of the north wall.

In Fig. 4.2-1 the temperature distribution of the front face is illustrated. The deviation of the colour at the edges from mean values of the image is caused by the detection limits of the scanner. Only some correlations are given between temperature distribution and results of the geological mapping (Fig. 4.2-2). Because no specific anomalies were measured, the

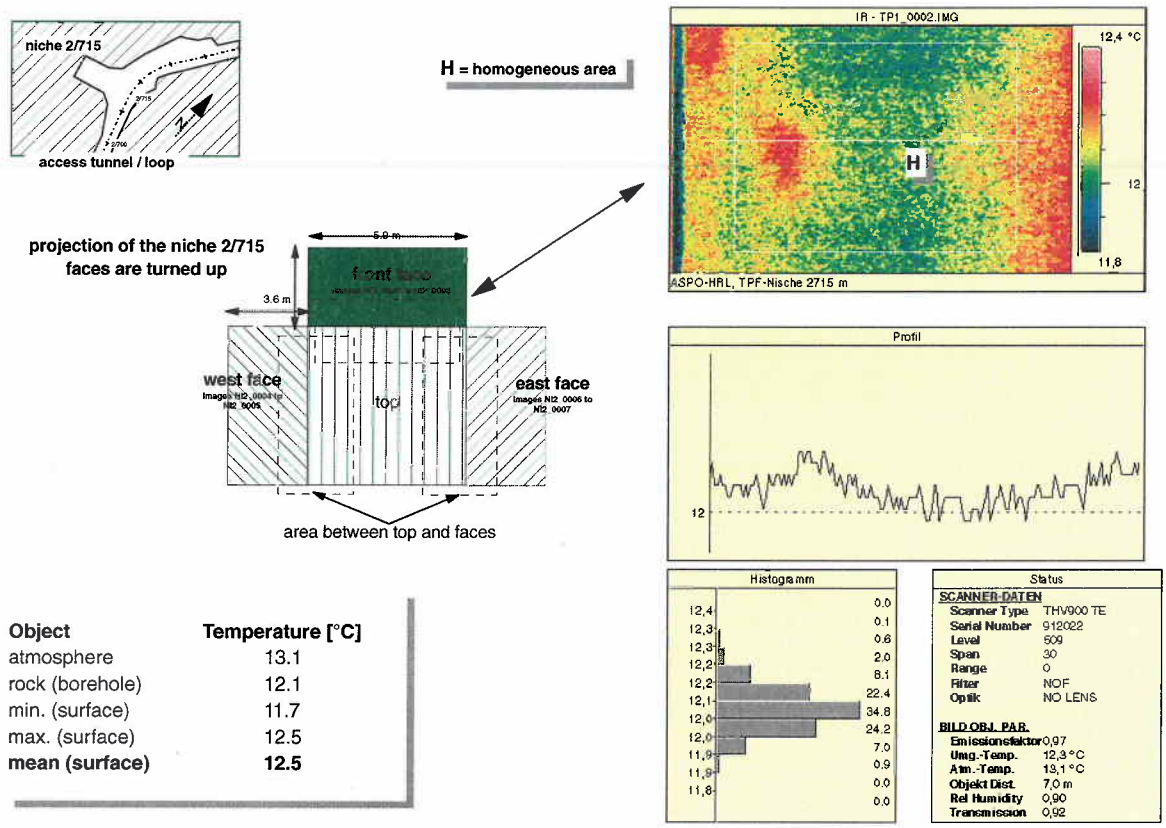

Object	Temperature [°C]
atmosphere	13.1
rock (borehole)	12.1
min. (surface)	11.7
max. (surface)	12.5
mean (surface)	**12.5**

Fig. 4.2-1 Geometry of the scanned area in the niche at tunnelmeter 2715. Temperature distribution at the center of the niche at tunnelmeter 2715 (profile, histogram, anomaly).

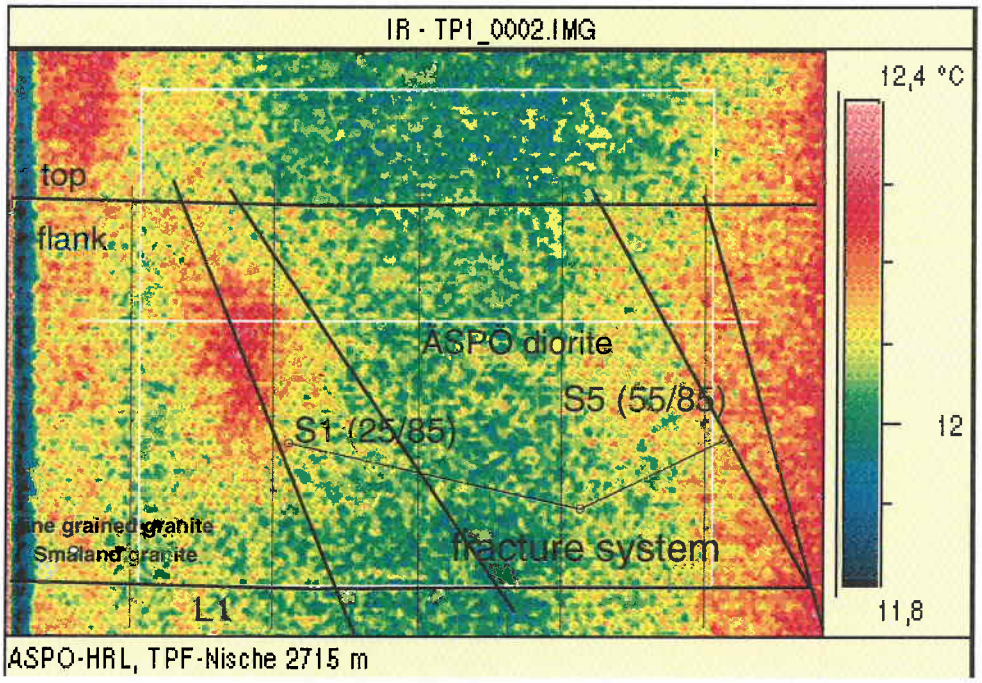

Fig. 4.2-2 Correlation of major hydraulic structures and temperature of the scanned area in the niche at tunnelmeter 2715.

temperature distribution can be considered as homogeneous. This lead to the interpretation that the front face is totally water saturated.

4.3 Conclusions

The geological mapping in the niche at tunnelmeter 2715 indicates different water-bearing structures. The rock mass temperature distribution was found to be homogeneous. The recent explanation of these two diverging results is that the rock is totally water saturated so evaporation is not effecting the temperature distribution of matrix areas.

Under consideration of the preliminary selection criteria, the results of the geological mapping lead to the conclusion that the location at tunnelmeter 2715 will be appropriate for the performance of the planned two-phase flow experiment. Especially with respect to the modeling part, the configuration of vertical and horizontal fractures in the near field of the niche guarantees well defined boundary conditions of the hydraulic flow field. The possible influence of artificial fractures on the flow field can be minimized by removal of the damaged front of the niche by additional smooth blasting.

5 Summary

In accordance with a BMBF/SKB-contract, a two-phase flow experiment (TPF) will be performed by GRS and BGR in the ÄSPÖ Hard Rock Laboratory (HRL) from 1997 to 1999. In preparation for this experiment, different in situ measurements were performed by GRS in 1996. Their objective was to test the applicability of envisaged measurement methods and to select a suitable underground test field.

The **analyses of** the mine air and of the formation water have shown that the **gases** released in detectable concentrations are hydrogen, methane, and carbon dioxide. Hydrogen was not found in the mine air, because it may possibly have escaped before sampling. The analyses of some samples of the mine air and of the formation water indicate that regions of much higher gas content exist; these may possibly correlate with mineralogical and stratigraphical rock properties, fissures, or tectonic fracture zones. Further investigations would be promising, because areas of higher gas content could indicate migration pathways for radionuclides.

Geoelectrical measurements were performed for investigating the excavation-disturbed zones (EDZ) and their desaturation around underground excavations. The disturbed zones around two drifts were investigated. One drift had been opened by drilling and blasting (D&B). The other had been mined by a tunnel boring machine. In the D&B drift it was found that the EDZ extends to a depth of 2.5 m. At the drift surface a strongly varying disturbed area of some centimeters to decimeters was found. In contrast, in the TBM drift the EDZ extends only to about 1 m. The quantification of the degree of desaturation of the disturbed zones would be possible on the basis of further laboratory calibration measurements on core samples from the investigated areas.

The **thermographic measurements** were performed in the D&B drift, in the TBM drift, in the niche at tunnelmeter 3170, in the access tunnel at tunnelmeter 1330, and in the niche designated for the TPF experiment at tunnelmeter 2715. At these locations the surface temperatures varied between 10.2 and 12.7 °C. The separately measured air temperatures ranged between 12 and 13.5 °C. In contrast to expectations, a homogeneous temperature distribution was found in some highly structured areas in the HRL. Obviously, these areas do not communicate with existing water-bearing systems. At some other locations, however, for instance in the TBM drift, a clear correlation between the temperature distribution and the

fracture system has been found. The thermographic method is therefore useful for identifying hydraulically active structures, even under the wet conditions in the HRL.

The **characterization of the TPF test field** was performed primarily on the basis of the thermographic measurements and geological mapping of the site. It was concluded that the location at tunnelmeter 2715 would be appropriate. With respect to modeling, the configuration of horizontal and vertical fractures provides well defined boundary conditions for the hydraulic flow field. The possible effect of excavation-induced fractures on the flow field will be reduced by removing the brittle front of the niche by additional smooth blasting.

6 References

/LOK 96/ Loke, M.H., Barker, R.D.
Rapid least-squares inversion of apparent resistivity pseudo-section by a quasi-Newton method.
Geophysical Prospecting 44, 131-152, 1996

/MAR 96/ Markström, I., Erlström, M.
Overview of Documentation of tunnel, niches and core boreholes.
SKB-PR 96/19, appendix D, p. 6, 1996

/OLS 96/ Olsson, O., Emsley, S., Bauer, C., Falls, S., Stenberg, L.
ZEDEX - A study of the zone of excavation disturbance for blasted and bored tunnels.
SKB-ICR 96/02 (vol. I - III), 1996

/YAR 92/ Yaramanci, U., Flach D.
Resistivity of rock salt in Asse (Germany) and petrophysical aspects.
Geophysical Prospecting 40, 85-100, 1992

/TEL 90/ Telford, W.M., Geldart, L.P. and Sheriff, R.E.
Applied Geophysics, 2nd Ed. Cambridge University Press, Cambridge 1990

/ZEL 96/ Zellman, O.
Personal Communication

Gesellschaft für Anlagen- und Reaktorsicherheit (GRS) mbH

Schwertnergasse 1
50667 Köln
Telefon +49 221 2068-0
Telefax +49 221 2068-888

Forschungsinstitute
85748 Garching b. München
Telefon +49 89 32004-0
Telefax +49 89 32004-300

Kurfürstendamm 200
10719 Berlin
Telefon +49 30 88589-0
Telefax +49 30 88589-111

Theodor-Heuss-Straße 4
38122 Braunschweig
Telefon +49 531 8012-0
Telefax +49 531 8012-200

www.grs.de

ISBN 3-931995-03-8